



Crystal structure of an anti-podoplanin antibody bound to a disialylated O-linked glycopeptide

Satoshi Ogasawara ^{a, b, *}, Kano Suzuki ^a, Kentaro Naruchi ^c, Seiya Nakamura ^a, Junpei Shimabukuro ^c, Nanase Tsukahara ^c, Mika K. Kaneko ^d, Yukinari Kato ^{d, e}, Takeshi Murata ^{a, b, **}

^a Graduate School of Science, Chiba University, Chiba, Japan

^b Molecular Chirality Research Center, Chiba University, Chiba, Japan

^c Medicinal Chemistry Pharmaceuticals, Co., Ltd., Sapporo, Japan

^d Tohoku University Graduate School of Medicine, Sendai, Japan

^e New Industry Creation Hatchery Center, Tohoku University, Sendai, Japan



ARTICLE INFO

Article history:

Received 26 August 2020

Accepted 27 August 2020

Available online 10 September 2020

Keywords:

Podoplanin (PDPN)

Monoclonal antibody

Crystal structure

Glycopeptide

ABSTRACT

Podoplanin (PDPN) is a highly O-glycosylated glycoprotein that is utilized as a specific lymphatic endothelial marker under pathophysiological conditions. We previously developed an anti-human PDPN (hPDPN) monoclonal antibody (mAb), clone LpMab-3, which recognizes the epitope, including both the peptides and the attached disialy-core-1 ($\text{NeuAc}\alpha\text{2-3Gal}\beta\text{l-3}[{\text{NeuAc}\alpha\text{2-6}]\text{GalNAc}\alpha\text{l-O-Thr}$) structure at the Thr76 residue in hPDPN. However, it is unclear if the mAb binds directly to both the peptides and glycans. In this study, we synthesized the binding epitope region of LpMab-3 that includes the peptide ($\text{-67LVATSVNSV-T-GIRIEDLP84-}$) possessing a disialyl-core-1 O-glycan at Thr76, and we determined the crystal structure of the LpMab-3 Fab fragment that was bound to the synthesized glycopeptide at a 2.8 Å resolution. The six amino acid residues and two sialic acid residues are directly associated with four complementarity-determining regions (CDRs; H1, H2, H3, and L3) and four CDRs (H2, H3, L1, and L3), respectively. These results suggest that IgG is advantageous for generating binders against spacious epitopes such as glycoconjugates.

© 2020 The Authors. Published by Elsevier Inc. This is an open access article under the CC BY license (<http://creativecommons.org/licenses/by/4.0/>).

1. Introduction

Podoplanin (PDPN) was previously discovered in renal podocytes [1], and it was recently reported as a novel biomarker of ischemia-reperfusion injury (IRI), as an increase in the urine PDPN-to-creatinine ratio is strongly correlated with the onset of renal IRI [2]. PDPN has also been reported to be expressed in lymphatic endothelial cells, but not in vascular endothelial cells [3,4]. Based on this, PDPN can be utilized as a specific lymphatic endothelial marker under pathophysiological conditions [5]. PDPN binds to the C-type lectin-like receptor-2 (CLEC-2) of platelets to induce platelet

aggregation [6,7]. PDPN was therefore previously referred to as “Aggrus” [8]. PDPN-CLEC-2 signaling leads to platelet aggregation, a process that is critical for embryonic blood-lymphatic vascular separation [9]. PDPN is also abundant in lung type I alveolar cells, where it is called as “T1 α ” [10]; however, it is not expressed in type II alveolar cells. Based on the use of PDPN as a specific marker for type I alveolar cells, the development and function of type I alveolar cells has been investigated in detail [11].

PDPN is also overexpressed in various tumors, including oral cancer, lung cancer, esophageal cancer, malignant brain tumors, mesotheliomas, testicular tumors, and osteosarcoma [8,12–21]. Number of reports have indicated that PDPN expression is associated with malignant progression and cancer metastasis [7,17], and PDPN expression is also associated with clinical outcomes [22]. PDPN has also been reported to be expressed by tumor-initiating cells (TICs) that are believed to be responsible for tumor relapse and resistance to conventional therapies [23].

25 years ago, Toyoshima et al. reported that mouse PDPN/gp44

* Corresponding author. Graduate School of Science, Chiba University, Chiba, Japan.

** Corresponding author. Graduate School of Science, Chiba University, Chiba, Japan.

E-mail addresses: satoshi-ogasawara@chiba-u.jp (S. Ogasawara), t.murata@faculty.chiba-u.jp (T. Murata).

is highly *O*-glycosylated and that this glycosylation is associated with platelet aggregation [24]. In our previous studies that examined the effect of glycosylation on platelet aggregation activity, recombinant podoplanins were expressed by Lec1 (lacking *N*-glycan), Lec2 (lacking sialic acid) and Lec8 (lacking galactose), such as glycosylation mutants of Chinese hamster ovary (CHO) cell [25]. PDPN treatment of Lec1 cells induced platelet aggregation; however, this was not observed in Lec2 and Lec8 cells. Lectin blot analyses suggested that sialylation of core-1 structures were critical for platelet aggregation activity [25]. Thus the activity was affected by the sialic acid and revivable by additional sialylation [26]. Additionally, a further analysis clarified that the Thr52 of human PDPN was glycosylated the disialyl-core-1 (*NeuAca2-3Galβ1-3(NeuAca2-6)GalNAc1-O-Thr*) structure [26]. These results indicated that the sialylated core-1 at Thr52 of human PDPN is critical for PDPN-induced platelet aggregation. To elucidate the structural basis of the glycan-dependent interactions between PDPN and CLEC-2, we performed crystallographic studies of PDPN in complex with CLEC-2 [27]. The interaction of human PDPN with CLEC-2 primarily involves Glu47 and Asp48 in the platelet aggregation-stimulating domain-3 (PLAG3) and the α-2, 6 linked sialic acid attached on Thr52 of human PDPN [27]. Interestingly, this PLAG domain is highly conserved among PDPNs of various species [28]. PLAG domains such as PLAG1, PLAG2, and PLAG3 are located within the N-terminus of PDPN [28], and PLAG-like domains (PLDs), also named PLAG4 [29], are found in the middle of PDPNs [30]. Although the disialyl-core-1 structure is attached within PLAG domains and PLDs and is primarily involved in PDPN-CLEC-2 interaction [7,29], the other Ser/Thr residues in PDPN may also possess *O*-glycans, as half of the molecular weight of PDPN is known to be derived from glycans [26]. The function of these *O*-glycans has not been clarified.

We have previously developed a number of monoclonal antibodies (mAbs) against human PDPN [15,31]. The binding epitopes of several anti-human PDPN mAbs were determined to include both peptides and glycans, including LpMab-2, LpMab-3, LpMab-9, LpMab-12, LpMab-19, and LpMab-21 [31–36], that were developed using Cancer-specific mAb (CasMab) technology [31]. We named this type of mAbs as anti-glycopeptide mAbs (GpMabs). Epitope mapping is typically performed using the alanine scanning method, and the binding epitope of LpMab-2 includes Thr55/Ser56, while the binding epitopes of LpMab-3, LpMab-19, and LpMab-21 include Thr76, that of LpMab-12 includes Thr52, and that of LpMab-9 includes Thr25. However, we have not clearly demonstrated if

GpMabs can directly react with both peptides and glycans. In this study, we first synthesized the PDPN-glycopeptide that included Thr76. We determined the crystal structure of a complex of LpMab-3-Fab and PDPN-glycopeptides, and our results revealed that the antibody directly binds to both peptides and glycans tightly.

2. Materials and Methods

2.1. Synthesis of the PDPN-glycopeptide

The PDPN-glycopeptide was synthesized in combination with a solid phase method and glycosyl transferase reaction. These methods were described in detail in Supporting Information.

2.2. Purification and crystallization of the Fab fragment

The papain (Nacalai Tesque, Inc., Kyoto, Japan) was immobilized on NHS-activated Sepharose 4 Fast Flow (GE Healthcare, Uppsala, Sweden). Purified LpMab-3 IgG was incubated with the immobilized papain in the presence of 2 mM cysteine-HCl and 20 mM EDTA in phosphate-buffered saline (PBS, pH 7.4) for 8 h at 37 °C under gentle agitation. After removing the immobilized papain, the reaction mixture was applied onto a pre-equilibrated rProtein A Sepharose Fast Flow column (GE Healthcare) with PBS containing 2.5 M NaCl. The flow-through fraction containing the Fab fragment was collected and concentrated, and this was further purified by performing gel filtration chromatography on a Superdex 200 10/300 column (GE Healthcare) equilibrated with PBS. The fractions containing the Fab fragment were collected and concentrated to 10–15 mg/mL. Crystallization trials were performed using the sitting-drop vapor diffusion method at 20 °C as described elsewhere [37]. The crystals were obtained by mixing 0.1 μL of purified sample with 0.1 μL of reservoir solution (0.1 M Tris-HCl [pH 7.5], 0.2 M magnesium-Acetate, and 25% [v/v] PEG-3350), and they were then soaked in cryoprotectant containing 20% (v/v) glycerol in crystallization buffer for a few minutes prior to flash freezing.

2.3. Co-crystallization of the Fab fragment and the PDPN-glycopeptide

The excess PDPN-glycopeptide was added to LpMab-3/Fab (molar ratio = 100:1) and incubated for 1 h at 4 °C. The unbound PDPN-glycopeptide was removed using a 10 MWCO Amicon-Ultra

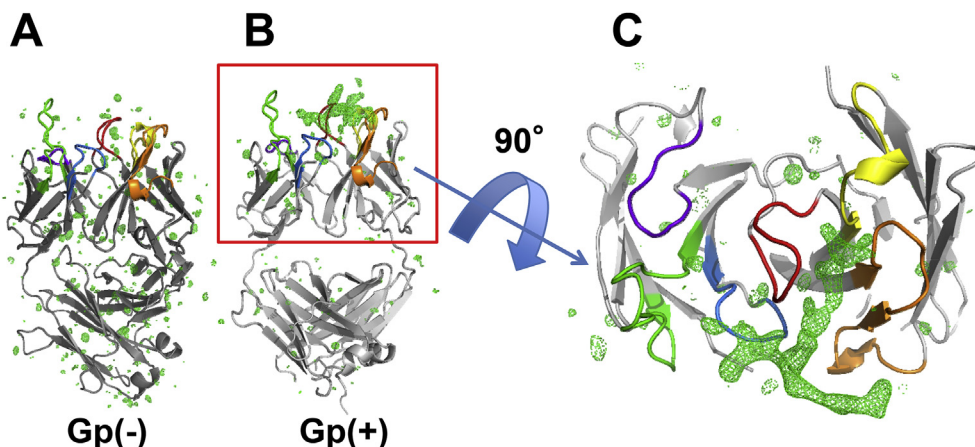


Fig. 1. Structures of LpMab-3 Fab fragment with/without PDPN-glycopeptide. Sections (A) and (B) show the overall structures of the LpMab-3 Fab fragment crystallized in the absence and presence of PDPN-glycopeptide, respectively. (C) Magnified top view of (B). The |Fo|-|Fc| electron density maps calculated without the glycopeptide contoured 3.0 σ are shown in green (positive) and red (negative). CDR-L1, CDR-L2, CDR-L3, CDR-H1, CDR-H2, and CDR-H3 regions of the antibody are colored in green, violet, blue, yellow, orange, and red, respectively.

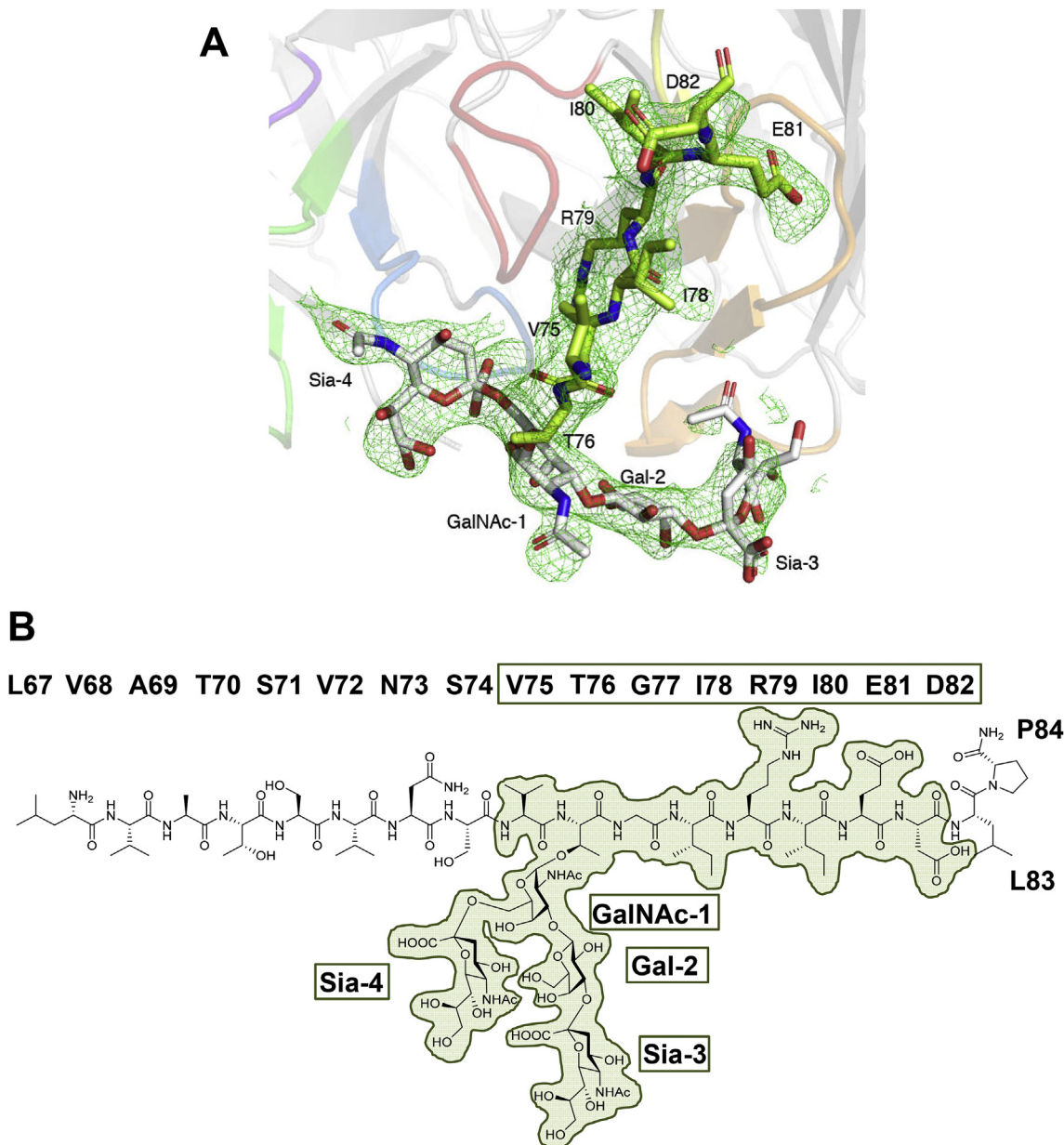


Fig. 2. Structure of the PDPN-glycopeptide. (A) Magnified view of the PDPN-glycopeptide within the crystal structure of the glycopeptide-bound LpMab-3 Fab fragment (shown as a stick model) with a positive electron density map (shown in green) calculated without the glycopeptide contouring 1.5σ . (B) Structural formula of the synthesized PDPN-glycopeptide. The highlighted area in green corresponds to that of the positive electron density map in (A).

(Merck Millipore) ultrafiltration device and then concentrated to 10–15 mg/mL. Crystallization trials were performed using the sitting-drop vapor diffusion method at 20 °C. The crystals were obtained by mixing 0.1 μL of purified sample with 0.1 μL of reservoir solution (0.1 M Tris-HCl [pH 7.5], 0.2 M magnesium-Acetate, and 25% [v/v] PEG-3350), and they were then soaked in cryoprotectant containing 20% (v/v) glycerol in crystallization buffer for a few minutes prior to flash freezing.

2.4. Structure determination

All X-ray diffraction data sets were collected from a single crystal at a cryogenic temperature (100 K). For LpMab-3/Fab bound with/without PDPN-glycopeptide, X-ray diffraction data sets were collected on a beamline BL-1A ($\lambda = 1.1 \text{ \AA}$) located at the Photon

Factory (Tsukuba, Japan). The collected data from LpMab-3/Fab bound without PDPN-glycopeptide were processed to 2.1 Å using XDS [38]. The structure was solved by molecular replacement with Phaser [39] using the antibody Fab fragment *exo* Diels-Alderase inhibitor complex (PDB ID: 1A3L) as a search model. The collected data from LpMab-3/Fab bound with PDPN-glycopeptide were processed to 2.8 Å using XDS [38]. The structure was solved by molecular replacement with Phaser [39] using the Diels-Alderase catalytic antibody Fab fragment (PDB ID: 1A4J; chains A and B) as a search model.

The atomic models were created manually using Coot [40] and refined iteratively using PHENIX [41]. RAMPAGE was used to validate the refined structures [42], and the crystallographic and refinement statistics are summarized in *Supplementary Table 1*. $\text{C}\alpha$ atoms were used for the calculation of all RMSD values. LigPlot⁺

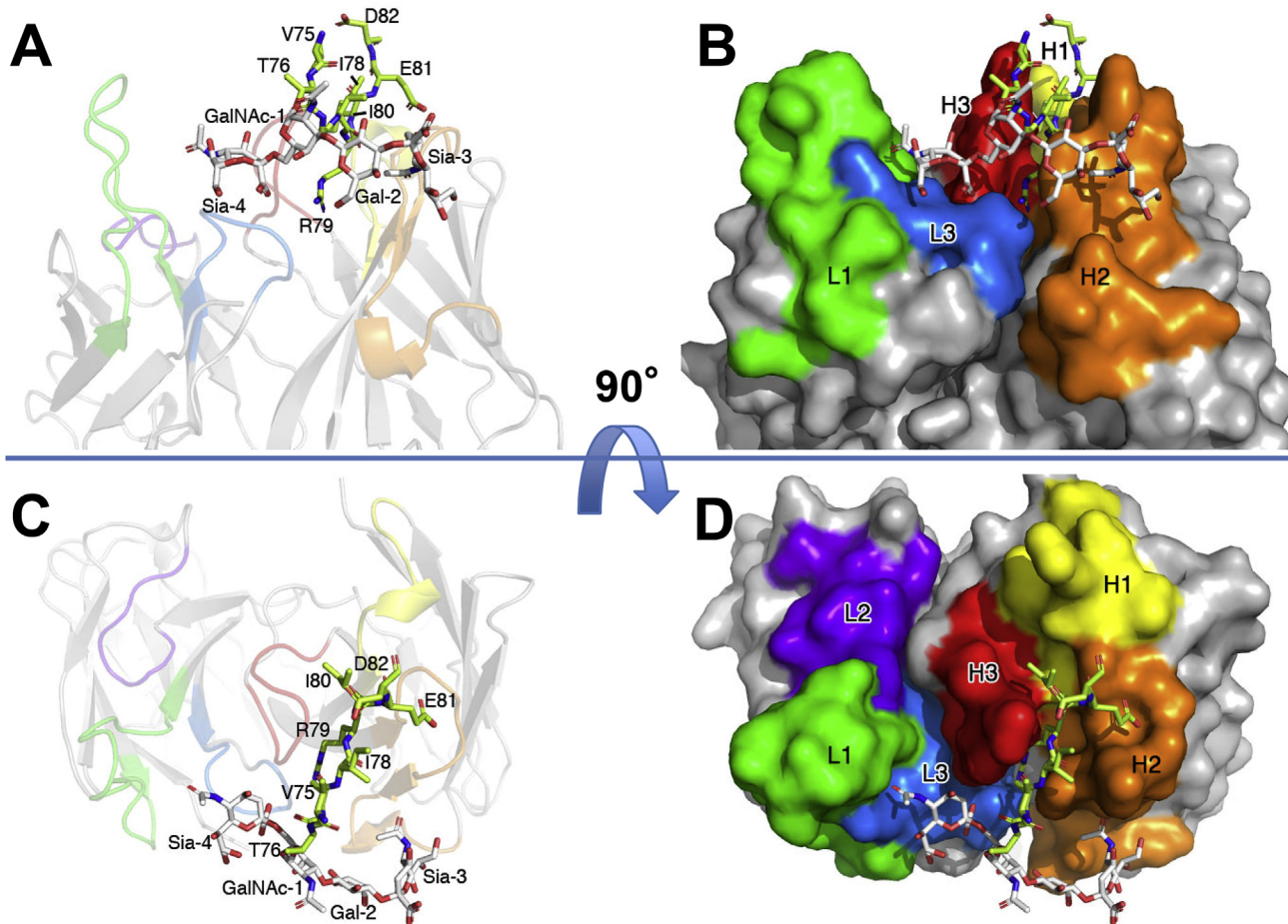


Fig. 3. Interactions between PDPN-glycopeptide and CDRs in LpMab-3. Side-view structures of PDPN-glycopeptide-bound Mab-3 Fab fragment corresponding to the red box in Fig. 3b. The Fab fragment is illustrated as a cartoon model (A) and surface model (B). The glycopeptide is presented as a stick model. The colors of the CDRs correspond to those in Fig. 1. (C) and (D) are the top-view structures of (A) and (B), respectively.

was used for the analysis of the glycopeptide-antibody interaction [43], and the figures were prepared using PyMOL (PyMOL Molecular Graphics System, version 2.1.1, Schrödinger LLC, New York, NY, USA).

3. Results

3.1. Synthesis of PDPN glycopeptide

We synthesized the PDPN-glycopeptide containing disialyl-core-1 at the Thr76 residue (Fig. S1) by using a solid phase method and enzymatic reaction. To distinguish two sialic acid residues in glycan, the sialic acid bound to galactose and the other bound to N-acetylgalactosamine denote as Sia-3 and Sia-4, respectively (Fig. S2A).

The binding ability of the synthesized PDPN-glycopeptide to the LpMab-3 antibody was evaluated using biolayer interferometry (BLItz system). The dissociation constant (K_D) value was estimated to be $2.0 \pm 0.5 \times 10^{-6}$ M (Fig. S2C), which was approximately 24-fold higher than the value estimated when using purified recombinant PDPN protein (K_D : 8.5×10^{-8} M) [35]. The lower binding affinity of the synthesized glycopeptide may be responsible for the higher fluctuation of the peptide portion. However, the K_D value of the glycopeptide appears to be sufficient to obtain the crystal structure of the complex.

3.2. Crystal structures of an antibody (LpMab-3) Fab fragment bound with/without the synthesized PDPN-glycopeptide

We purified the Fab fragment of LpMab-3 using a Protein A column and gel filtration chromatographies after papain treatment (see Materials and Methods), and we crystallized and determined the crystal structure at a resolution of 2.1 Å (PDB ID: 7C95; Table S1). Two Fab fragments were present within the asymmetric unit of the crystal lattice. The structures of the variable (Fv) regions closely resembled each other (Ca root-mean-square deviation [RMSD] = 0.61 Å). Fig. 1A shows a Fab fragment (chains A and B) with an $F|o| - F|c|$ electron density map. No significant positive electron density was observed surrounding the CDR regions. Next, we crystallized the Fab fragment in the presence of an excess concentration of the synthesized PDPN-glycopeptide and obtained an electron density map at a resolution of 2.8 Å (PDB ID: 7C94; Table S1). This crystal also contained two antibody fragments within the asymmetric unit. After Fab fragment molecules were fitted into the density, strong positive electron densities that are interpreted as glycopeptides were observed surrounding the CDRs of the antibodies (Fig. 3B). We modeled eight amino acid residues (VTGIRIED) and the disialyl-core-1 structure of the glycopeptide by guiding the shape of the electron density map (Fig. 2). There was no significant electron density for the N-terminal amino acid residues (LVATSVNS) located upstream of Val75 or the C-terminal amino acid residues (LP) located downstream of Asp82 in the

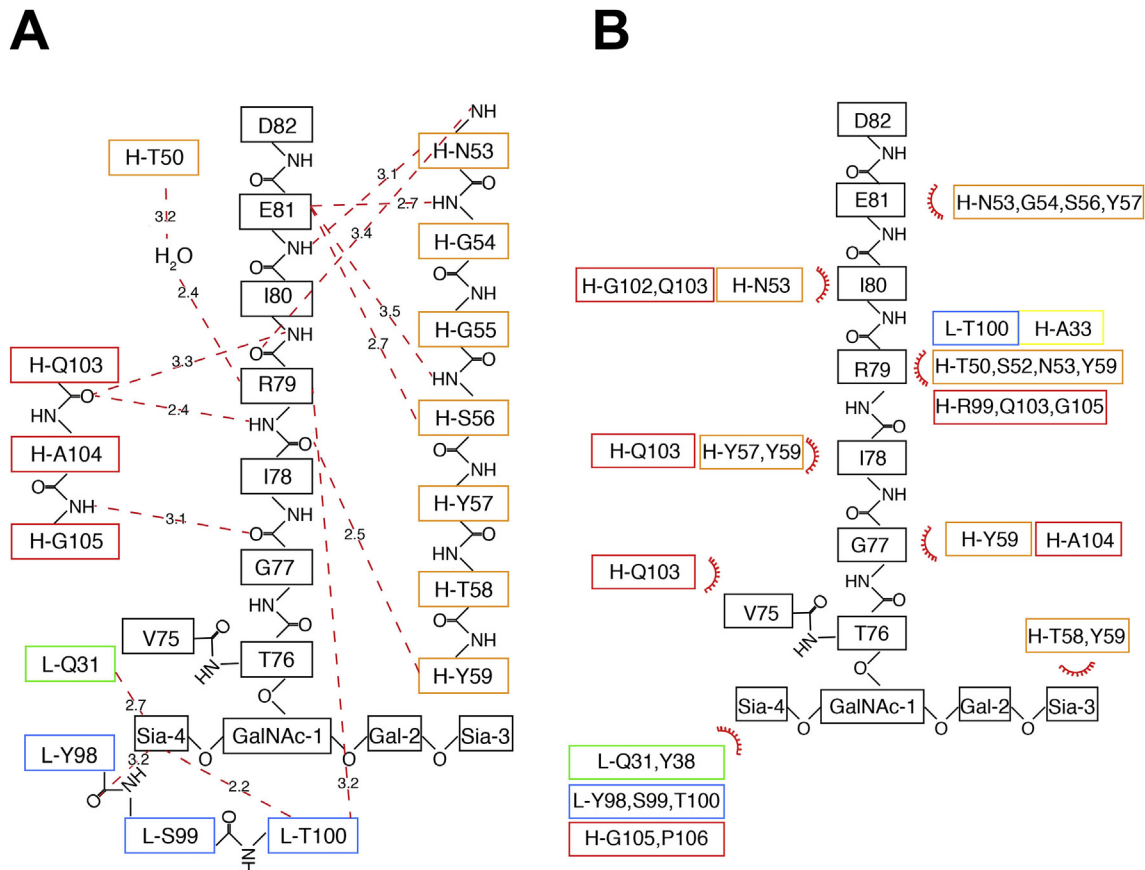


Fig. 4. Schematic representation of the interactions between PDPN-glycopeptide and CDRs in LpMab-3. The distances separating the amino acid residues in LpMab-3 Fab and the PDPN-glycopeptide were analyzed using the Ligplot⁺ program. (A) Hydrogen bonds are shown as red dashed lines. The bond length cut off is set to 3.5 Å for hydrogen bond. (B) Van der Waals contacts are represented by the spoked arcs oriented toward the ligand atoms they contact. The range of distances defining van der Waals contacts is 2.9–3.9 Å. The colors of the CDRs correspond to those in Fig. 1.

glycopeptide, and this suggests that these residues do not bind to the antibody and are disordered. The observed eight amino acid residues and glycans are also indicated as the epitope region of PDPN for LpMab-3 by biochemical epitope mapping using the alanine scanning method [35]. The obtained structures of two Fab fragment molecules bound to the glycopeptide in the asymmetric unit were nearly identical ($\text{RMSD} = 0.31 \text{ \AA}$). Therefore, we used the data for a Fab fragment (chains A–C) in all of the figures and in the following discussion.

3.3. Binding interactions of the glycopeptide with LpMab-3

The eight amino acid residues (VTGIRIED) of the glycopeptide are located at the cavity between CDR-H2 and CDR-H3 that is formed by 11 hydrogen bonds and 22 van der Waals contacts (Figs. 3 and 4). Arg79 and Glu81 residues primarily contribute to these interactions, while the Thr76 that links the disialyl-core-1 glycan does not interact with the antibody. The disialyl-core-1 glycan is located on the surface of CDRs L3 and H2 that is formed by three hydrogen bonds and nine van der Waals contacts (Figs. 3 and 4). In particular, the α -2, 6 linked sialic acid residue (Sia-4) contributes to the majority of the interaction with the antibody. The other sialic acid residue (Sia-3) interacts with CDR-H2 Thr58 and Tyr59. The rest of the reduced saccharides (GalNAc-1 and Gal-2) do not interact with the antibody. Thus, the antibody LpMab-3 directly associates with six amino acid residues and two sialic acid residues.

4. Discussion

In this study, we first synthesized a disialylated O-linked glycopeptide, and we then determined the crystal structure of a complex of LpMab-3-Fab and the glycopeptide. To our knowledge, this is the first 3D structure of a complex between an antibody and a disialyl-core-1 linked glycopeptide. The structure of LpMab-3 reveals that five of six complementarity-determining regions (CDRs) are used to bind the glycopeptide. The peptide region of the glycopeptide interacts with CDRs of the heavy chain, and the glycan region is primarily associated with the CDRs of the light chain. Large antigens such as glycopeptides are difficult to recognize as an epitope using single-domain antibodies; however, this is possible using IgG-type antibodies. This property of IgG provides the potential to generate high specific mAbs against various types of glycopeptides.

Importantly, this antibody directly binds to two sialic acid residues of the disialyl-core-1 structure. It is generally established that the sialic acid residues of the glycans are involved in facilitating influenza virus infections [44,45], the toxicity of cobra toxin [46] or botulinum toxin [47], the parasitism of malarial parasites [48], and in other processes. This structural information that allows for the recognition of sialic acid by antibodies may be useful for designing neutralizing antibodies that function to bind sialic acid to provide protection from these biological hazards.

Author contributions

S.O., Y.K. and T.M. conceived and designed the study. S.O. and M.K.K. prepared protein sample. M.K.K. sequenced the gene of antibody. N.K., J.S. and N.T. synthesized the glycopeptide. S.O. and S.N. analyzed the binding affinity. S.O. and K.S. performed the crystallization. K.S., S.N. and T.M. processed and refined x-ray data. S.O., N.K., Y.K. and T.M. wrote the paper. All authors read and approved the manuscript.

Accession codes

Coordinates and structure factors have been deposited in the Protein Data Bank under accession codes 7C94 (LpMab-3-Fab with PDPN-glycopeptide) and 7C95 (LpMab-3-Fab without PDPN-glycopeptide).

Funding

This research was supported in part by Japan Agency for Medical Research and Development (AMED) under Grant nos. JP20am0101083 (T.M.), JP20am0101078 (Y.K.), JP20am0401013 (Y.K.) and JP20ae0101028 (Y.K.), and by Grant-in-Aid for Scientific Research from Japan Society for the Promotion of Science (JSPS) under Grant nos. 18H05425 (T.M.), 17K07299 (M.K.K.), and 19K07705 (Y.K.).

Declaration of competing interest

The authors declare that they have no known competing financial interests or personal relationships that could have appeared to influence the work reported in this paper.

Acknowledgments

The synchrotron radiation experiments were performed at Photon Factory (proposals 2018G120 and 2018RP-16). We thank the beamline staff at BL1A of Photon Factory (Tsukuba, Japan) for help during data collection.

Appendix A. Supplementary data

Supplementary data to this article can be found online at <https://doi.org/10.1016/j.bbrc.2020.08.103>.

References

- [1] S. Breiteneder-Geleff, K. Matsui, A. Soleiman, P. Meraner, H. Poczewski, R. Kalt, G. Schaffner, D. Kerjaschki, Podoplanin, novel 43-kd membrane protein of glomerular epithelial cells, is down-regulated in puromycin nephrosis, *Am. J. Pathol.* 151 (1997) 1141–1152.
- [2] V. Kasinath, O.A. Yilmam, M. Uehara, M. Yonar, L. Jiang, X. Li, W. Qiu, S. Eskandari, T. Ichimura, R. Abdi, Urine podoplanin heralds the onset of ischemia-reperfusion injury of the kidney, *Am. J. Physiol. Ren. Physiol.* 316 (2019) F957–F965.
- [3] S. Breiteneder-Geleff, A. Soleiman, H. Kowalski, R. Horvat, G. Amann, E. Kriehuber, K. Diem, W. Weninger, E. Tschachler, K. Alitalo, et al., Angiosarcomas express mixed endothelial phenotypes of blood and lymphatic capillaries: podoplanin as a specific marker for lymphatic endothelium, *Am. J. Pathol.* 154 (1999) 385–394.
- [4] V. Schacht, S.S. Dadras, L.A. Johnson, D.G. Jackson, Y.K. Hong, M. Detmar, Up-regulation of the lymphatic marker podoplanin, a mucin-type transmembrane glycoprotein, in human squamous cell carcinomas and germ cell tumors, *Am. J. Pathol.* 166 (2005) 913–921.
- [5] E. Jung, D. Gardner, D. Choi, E. Park, Y. Jin Seong, S. Yang, J. Castorena-Gonzalez, A. Louveau, Z. Zhou, G.K. Lee, et al., Development and characterization of a novel prox1-EGFP lymphatic and schlemm's canal reporter rat, *Sci. Rep.* 7 (2017) 5577.
- [6] K. Suzuki-Inoue, Y. Kato, O. Inoue, M.K. Kaneko, K. Mishima, Y. Yatomi, Y. Yamazaki, H. Narimatsu, Y. Ozaki, Involvement of the snake toxin receptor CLEC-2, in podoplanin-mediated platelet activation, by cancer cells, *J. Biol. Chem.* 282 (2007) 25993–26001.
- [7] Y. Kato, M.K. Kaneko, A. Kunita, H. Ito, A. Kameyama, S. Ogasawara, N. Matsuura, Y. Hasegawa, K. Suzuki-Inoue, O. Inoue, et al., Molecular analysis of the pathophysiological binding of the platelet aggregation-inducing factor podoplanin to the C-type lectin-like receptor CLEC-2, *Canc. Sci.* 99 (2008) 54–61.
- [8] Y. Kato, N. Fujita, A. Kunita, S. Sato, M. Kaneko, M. Osawa, T. Tsuruo, Molecular identification of Aggrus/T1alpha as a platelet aggregation-inducing factor expressed in colorectal tumors, *J. Biol. Chem.* 278 (2003) 51599–51605.
- [9] C.C. Bertozzi, A.A. Schmaier, P. Mericko, P.R. Hess, Z. Zou, M. Chen, C.Y. Chen, B. Xu, M.M. Lu, D. Zhou, et al., Platelets regulate lymphatic vascular development through CLEC-2-SLP-76 signaling, *Blood* 116 (2010) 661–670.
- [10] A.K. Rishi, M. Joyce-Brady, J. Fisher, L.G. Dobbs, J. Floros, J. VanderSpek, J.S. Brody, M.C. Williams, Cloning, characterization, and development expression of a rat lung alveolar type I cell gene in embryonic endodermal and neural derivatives, *Dev. Biol.* 167 (1995) 294–306.
- [11] R. Gonzalez, D. Leaffer, C. Chapin, A.M. Gillespie, W. Eckalbar, L. Dobbs, Cell fate analysis in fetal mouse lung reveals distinct pathways for T1 and TII cell development, *Am. J. Physiol. Lung Cell Mol. Physiol.* 317 (2019) L653–L666.
- [12] Y. Kato, I. Sasagawa, M. Kaneko, M. Osawa, N. Fujita, T. Tsuruo, Aggrus: a diagnostic marker that distinguishes seminoma from embryonal carcinoma in testicular germ cell tumors, *Oncogene* 23 (2004) 8552–8556.
- [13] E. Martin-Villar, F.G. Scholl, C. Gamallo, M.M. Yurrita, M. Munoz-Guerra, J. Cruces, M. Quintanilla, Characterization of human PA2.26 antigen (T1alpha-2, podoplanin), a small membrane mucin induced in oral squamous cell carcinomas, *Int. J. Canc.* 113 (2005) 899–910.
- [14] Y. Kato, M. Kaneko, M. Sata, N. Fujita, T. Tsuruo, M. Osawa, Enhanced expression of Aggrus (T1alpha/podoplanin), a platelet-aggregation-inducing factor in lung squamous cell carcinoma, *Tumor Biol.* 26 (2005) 195–200.
- [15] Y. Kato, M.K. Kaneko, A. Kuno, N. Uchiyama, K. Amano, Y. Chiba, Y. Hasegawa, J. Hirabayashi, H. Narimatsu, K. Mishima, et al., Inhibition of tumor cell-induced platelet aggregation using a novel anti-podoplanin antibody reacting with its platelet-aggregation-stimulating domain, *Biochem. Biophys. Res. Commun.* 349 (2006) 1301–1307.
- [16] K. Mishima, Y. Kato, M.K. Kaneko, Y. Nakazawa, A. Kunita, N. Fujita, T. Tsuruo, R. Nishikawa, T. Hirose, M. Matsutani, Podoplanin expression in primary central nervous system germ cell tumors: a useful histological marker for the diagnosis of germinoma, *Acta Neuropathol.* 111 (2006) 563–568.
- [17] K. Mishima, Y. Kato, M.K. Kaneko, R. Nishikawa, T. Hirose, M. Matsutani, Increased expression of podoplanin in malignant astrocytic tumors as a novel molecular marker of malignant progression, *Acta Neuropathol.* 111 (2006) 483–488.
- [18] S. Abe, Y. Morita, M.K. Kaneko, M. Hanibuchi, Y. Tsujimoto, H. Goto, S. Kakuchi, Y. Aono, J. Huang, S. Sato, et al., A novel targeting therapy of malignant mesothelioma using anti-podoplanin antibody, *J. Immunol.* 190 (2013) 6239–6249.
- [19] A. Kunita, T.G. Kashima, A. Ohazama, A.E. Grigoriadis, M. Fukayama, Podoplanin is regulated by AP-1 and promotes platelet aggregation and cell migration in osteosarcoma, *Am. J. Pathol.* 179 (2011) 1041–1049.
- [20] Y. Kato, G. Vaideyanathan, M.K. Kaneko, K. Mishima, N. Srivastava, V. Chandramohan, C. Pegram, S.T. Keir, C.T. Kuan, D.D. Bigner, et al., Evaluation of anti-podoplanin rat monoclonal antibody NZ-1 for targeting malignant gliomas, *Nucl. Med. Biol.* 37 (2010) 785–794.
- [21] A. Kunita, T.G. Kashima, Y. Morishita, M. Fukayama, Y. Kato, T. Tsuruo, N. Fujita, The platelet aggregation-inducing factor aggrus/podoplanin promotes pulmonary metastasis, *Am. J. Pathol.* 170 (2007) 1337–1347.
- [22] P. Yuan, S. Temam, A. El-Naggar, X. Zhou, D. Liu, J. Lee, L. Mao, Overexpression of podoplanin in oral cancer and its association with poor clinical outcome, *Cancer* 107 (2006) 563–569.
- [23] N. Atsumi, G. Ishii, M. Kojima, M. Sanada, S. Fujii, A. Ochiai, Podoplanin, a novel marker of tumor-initiating cells in human squamous cell carcinoma A431, *Biochem. Biophys. Res. Commun.* 373 (2008) 36–41.
- [24] M. Toyoshima, M. Nakajima, T. Yamori, T. Tsuruo, Purification and characterization of the platelet-aggregating sialoglycoprotein gp44 expressed by highly metastatic variant cells of mouse colon adenocarcinoma 26, *Canc. Res.* 55 (1995) 767–773.
- [25] M. Kaneko, Y. Kato, A. Kunita, N. Fujita, T. Tsuruo, M. Osawa, Functional sialylated O-glycan to platelet aggregation on Aggrus (T1alpha/podoplanin) molecules expressed in Chinese Hamster Ovary cells, *J. Biol. Chem.* 279 (2004) 38838–38843.
- [26] M.K. Kaneko, Y. Kato, A. Kameyama, H. Ito, A. Kuno, J. Hirabayashi, T. Kubota, K. Amano, Y. Chiba, Y. Hasegawa, et al., Functional glycosylation of human podoplanin: glycan structure of platelet aggregation-inducing factor, *FEBS Lett.* 581 (2007) 331–336.
- [27] M. Nagae, K. Morita-Matsumoto, M. Kato, M.K. Kaneko, Y. Kato, Y. Yamaguchi, A Platform of C-Type lectin-like receptor CLEC-2 for binding O-glycosylated podoplanin and nonglycosylated rhodocytin, *Structure* 22 (2014) 1711–1721.
- [28] M.K. Kaneko, Y. Kato, T. Kitano, M. Osawa, Conservation of a platelet activating domain of Aggrus/podoplanin as a platelet aggregation-inducing factor, *Gene* 378 (2006) 52–57.
- [29] T. Sekiguchi, A. Takemoto, S. Takagi, K. Takatori, S. Sato, M. Takami, N. Fujita, Targeting a novel domain in podoplanin for inhibiting platelet-mediated tumor metastasis, *Oncotarget* 7 (2015) 3934–3946.
- [30] Y. Sayama, M. Sano, T. Asano, Y. Furusawa, J. Takei, T. Nakamura, M. Yanaka,

- S. Okamoto, S. Handa, Y. Komatsu, Y. Nakamura, M. Yanagawa, M.K. Kaneko, Y. Kato, Epitope mapping of PMab-241, a lymphatic endothelial cell-specific anti-bear podoplanin monoclonal antibody, *Monoclon. Antibodies Immunodiagn. Immunother.* 39 (2020) 77–81.
- [31] Y. Kato, M.K. Kaneko, A cancer-specific monoclonal antibody recognizes the aberrantly glycosylated podoplanin, *Sci. Rep.* 4 (2014) 5924.
- [32] Y. Kato, S. Ogasawara, H. Oki, P. Goichberg, R. Honma, Y. Fujii, M.K. Kaneko, LpMab-12 established by CasMab technology specifically detects sialylated O-glycan on Thr52 of platelet aggregation-stimulating domain of human podoplanin, *PLoS One* 11 (2016), e0152912.
- [33] M.K. Kaneko, H. Oki, Y. Hozumi, X. Liu, S. Ogasawara, M. Takagi, K. Goto, Y. Kato, Monoclonal antibody LpMab-9 recognizes O-glycosylated N-terminus of human podoplanin, *Monoclon. Antibodies Immunodiagn. Immunother.* 34 (2015) 310–317.
- [34] S. Ogasawara, M.K. Kaneko, Y. Kato, LpMab-19 recognizes sialylated O-glycan on Thr76 of human podoplanin, *Monoclon. Antibodies Immunodiagn. Immunother.* 35 (2016) 245–253.
- [35] H. Oki, S. Ogasawara, M.K. Kaneko, M. Takagi, M. Yamauchi, Y. Kato, Characterization of monoclonal antibody LpMab-3 recognizing sialylated glycopeptide of podoplanin, *Monoclon. Antibodies Immunodiagn. Immunother.* 34 (2015) 44–50.
- [36] M.K. Kaneko, T. Nakamura, R. Honma, S. Ogasawara, Y. Fujii, S. Abe, M. Takagi, H. Harada, H. Suzuki, Y. Nishioka, et al., Development and characterization of anti-glycopeptide monoclonal antibodies against human podoplanin, using glycan-deficient cell lines generated by CRISPR/Cas9 and TALEN, *Cancer Med* 6 (2017) 382–396.
- [37] S. Maruyama, K. Suzuki, M. Imamura, H. Sasaki, H. Matsunami, K. Mizutani, Y. Saito, F.L. Imai, Y. Ishizuka-Katsura, T. Kimura-Someya, M. Shirouzu, T. Uchihashi, T. Ando, I. Yamato, T. Murata, Metastable asymmetric structure of a shaftless V1 motor, *Sci. Adv.* 5 (2019), eaau8149.
- [38] W. Kabsch, XDS, *Acta Crystallogr. Sect. D Biol. Crystallogr.* 66 (2010) 125–132.
- [39] A.J. McCoy, R.W. Grosse-Kunstleve, P.D. Adams, M.D. Winn, L.C. Storoni, R.J. Read, Phaser crystallographic software, *J. Appl. Crystallogr.* 40 (2007) 658–674.
- [40] P. Emsley, K. Cowtan, Coot: model-building tools for molecular graphics, *Acta Crystallogr. Sect. D Biol. Crystallogr.* 60 (2004) 2126–2132.
- [41] P.D. Adams, P.V. Afonine, G. Bunkoczi, V.B. Chen, I.W. Davis, N. Echols, J.J. Headd, L.-W. Hung, G.J. Kapral, R.W. Grosse-Kunstleve, A.J. McCoy, N.W. Moriarty, R. Oeffner, R.J. Read, D.C. Richardson, J.S. Richardson, T.C. Terwilliger, P.H. Zwart, PHENIX: a comprehensive Python-based system for macromolecular structure solution, *Acta Crystallogr. Sect. D Biol. Crystallogr.* 66 (2010) 213–221.
- [42] S.C. Lovell, I.W. Davis, W.B. Arendall III., P.I.W. de Bakker, J.M. Word, M.G. Prisant, J.S. Richardson, D.C. Richardson, Structure validation by $\text{C}\alpha$ geometry: ϕ, ψ and $\text{C}\beta$ deviation, *Proteins Struct. Funct. Genet.* 50 (2003) 437–450.
- [43] R.A. Laskowski, M.B. Swindells, LigPlot⁺: multiple ligand-protein interaction diagrams for drug discovery, *J. Chem. Inf. Model.* 51 (2011) 2778–2786.
- [44] Y. Suzuki, T. Nakao, T. Ito, N. Watanabe, Y. Toda, G. Xu, T. Suzuki, T. Kobayashi, Y. Kimura, A. Yamada, et al., Structural determination of gangliosides that bind to influenza A, B, and C viruses by an improved binding assay: strain-specific receptor epitopes in sialo-sugar chains, *Virology* 189 (1992) 121–131.
- [45] R. Wagner, M. Matrosovich, H.D. Klenk, Functional balance between haemagglutinin and neuraminidase in influenza virus infections, *Rev. Med. Virol.* 12 (2002) 159–166.
- [46] D.C. Gowda, E.A. Davidson, Structural features of carbohydrate moieties in snake venom glycoproteins, *Biochem. Biophys. Res. Commun.* 182 (1992) 294–301.
- [47] K. Niwa, T. Yoneyama, H. Ito, M. Taira, T. Chikai, H. Kouuchi, T. Suzuki, K. Hasegawa, K. Miyata, K. Inui, T. Ikeda, T. Watanabe, T. Ohyama, Sialic acid-dependent binding and transcytosis of serotype D botulinum neurotoxin and toxin complex in rat intestinal epithelial cells, *Vet. Microbiol.* 141 (2010) 312–320.
- [48] V.K. Goel, X. Li, H. Chen, S.C. Liu, A.H. Chishti, S.S. Oh, Band 3 is a host receptor binding merozoite surface protein 1 during the *Plasmodium falciparum* invasion of erythrocytes, *Proc. Natl. Acad. Sci. U.S.A.* 100 (2003) 5164–5169.